Journal of
Composites Science

MDPI

Article

Use of Dregs as a Replacement for Hydrated Lime in Cement Coating Mortar

Alencar Ibeiro de Oliveira [1], Mahbube Subhani [2,*], Arthur Behenck Aramburu [3], Hebert Luis Rossetto [1,4], Guilherme Höehr Trindade [4], White José dos Santos [5] and Rafael de Avila Delucis [1,4]

1 Postgraduation Program in Materials Science and Engineering, Federal University of Pelotas, Pelotas 96010-610, Brazil
2 School of Engineering, Deakin University, Waurn Ponds, VIC 3217, Australia
3 Postgraduation Program in Mining, Metallurgical and Materials Engineering, Federal University of Rio Grande do Sul, Porto Alegre 91509-900, Brazil
4 Graduate Program in Civil Engineering, Engineering Center, Federal University of Pelotas, Pelotas 96010-610, Brazil
5 Department of Materials Engineering and Civil Construction, Federal University of Minas Gerais, Belo Horizonte 31270-901, Brazil
* Correspondence: mahbube.subhani@deakin.edu.au

Abstract: The pulp and paper industry generates a significant volume of solid waste during its operations. In order to mitigate the environmental impact caused by this industry, one of its residues was applied in eco-friendly composites. Therefore, this research aims to use green liquor dregs as a partial replacement for lime in coating mortars. Hydrated lime was replaced by dregs in percentages of 10%, 15%, 20%, and 30%, and the manufactured mortar specimens were tested in terms of their flowability, air content, and specific gravity in the fresh state. In the hardened state, physical and chemical characterization was carried out to determine the influence of the introduction of the dregs on the properties of the different types of mortar. Mechanical testing of the mortar specimens' compressive, flexural, and adhesive strengths was carried out, and scanning electron microscopy was performed to evaluate the microstructural features of the cement composites. In general, the types of mortar with dregs showed a high degree of similarity to conventional mortar in all studied aspects, including the 30% replacement group. The obtained SEM images indicated that the presence of dregs in the mortar did not change the formational mechanism of C-S-H crystals, maintaining the mechanical properties of the material even after the accelerated aging procedure was performed, reaching similar levels of flexural, compressive, and tensile bond strengths when compared to the neat mortar. Furthermore, tensile bond levels reached approximately 0.9 MPa for all the studied types of mortar, allowing the material to be used in external applications.

Keywords: dregs; cement; mortar; lime; residue

Citation: de Oliveira, A.I.; Subhani, M.; Aramburu, A.B.; Rossetto, H.L.; Trindade, G.H.; dos Santos, W.J.; de Avila Delucis, R. Use of Dregs as a Replacement for Hydrated Lime in Cement Coating Mortar. *J. Compos. Sci.* **2023**, *7*, 181. https://doi.org/10.3390/jcs7050181

Academic Editor: Francesco Tornabene

Received: 30 March 2023
Revised: 17 April 2023
Accepted: 20 April 2023
Published: 1 May 2023

1. Introduction

The use of planted forests instead of native forests reduces the environmental impact of the pulp and paper sector, which is fundamental for the Brazilian national economy, however, this industrial activity is associated with environmental problems due to the significant volume of solid waste and effluents that are generated. Accordingly, many companies seek to achieve a circular economy incorporating this waste into products [1]. This circular economy is even more important in countries such as Brazil, which is one of the largest pulp exporters in the world and is among the top 10 countries in the world in terms of paper manufacturing, with 10.2 million tons produced in 2020 [2].

In this context, the kraft pulping method involves the generation of various types of waste, including ash, dregs, grit, and lime mud. Companies that use the kraft process have sought to use the waste by burning to generate energy, soil management, composting,

among other possibilities. However, the incorporation of this waste into construction materials would be an application with greater added value [3,4]. This is also an alternative to mitigate the environmental footprint of building materials [5,6], thus helping to preserve natural resources and reduce the emission of CO_2 into the atmosphere.

Regarding building materials, the performance of recycled waste aggregates is often inferior to the performance of natural aggregates, and the mixture of recycled aggregate negatively impacts the rheological properties, mechanical performance, and durability of cement composites; however, recent research has proven that good results can also be achieved [7,8]. In this regard, lime is produced from limestone through a process called calcination and has a major role in mortar as a source of calcium hydroxides ($Ca(OH)_2$). In fact, lime benefits mortar by retaining water and releasing it gradually, thereby increasing the hydration of the cement in later ages. Moreover, its addition also generates greater yields and increases mass volume and is associated with gains in workability, reduced permeability, and the prevention of fissures and cracks. Since lime is thinner than cement, it can still fill voids and accelerate the curing of cementitious composites through the carbonation process (calcium carbonate formation). However, it is estimated that the production of 1000 kg of CaO/MgO emits between 750 and 850 kg of CO_2, which includes the steps of raw material extraction, processing, and transport [9]. Thus, lime has recently been slowly replaced by modern additives capable of enhancing workability. However, lime is still the major material used for thus end in coating mortar.

To mitigate both the impacts generated by the pulping process and the CO_2 generated in limestone calcination, the partial replacement of lime with the solid waste of the kraft process in coating mortar may furnish an alternative construction material with great social interest, reducing both the environmental impact and the ultimate price of the final product. Green liquor dregs consist of undissolved particles composed of different inorganic oxides, which are formed in the process of recovering inorganic materials from green liquor after the black liquor evaporation and burning processes [1]. This residue remains unexplored on an industrial scale, however, several studies have aimed out management alternatives in various sectors, such as the construction material industry [10].

In civil construction, dregs have been used in a wide range of applications, including as fillers in asphalt mixtures [11] and in the creation of clinker for cement manufacturing [12]. A paper studying this topic was that written by Azevedo [4], wherein mixed mortar specimens were produced, replacing lime (20%) with green liquor dregs. This paper focuses more on environmental parameters, which show excellent results when lime is replaced with dregs. However, this study does not examine the variation of content or microstructural properties. Thus, the present study concerns the production and characterization of mixed coating mortar without additives with the partial replacement of hydrated lime by green liquor dregs with different replacement levels (10, 15, 20, and 30%) to increase the environmental appeal of this type of mortar. We evaluate the properties in the fresh and hardened state, the durability, and the microstructure of the coating mortar specimens.

2. Materials and Methods

2.1. Materials Selection and Characterization

CPII-F40 cement supplied by Votorantim Cimentos was used, and the specifications supplied by the manufacturer are shown in Table 1. This cement is suitable for use in coating mortar in accordance with NBR 16697 [13] and has a high degree of fineness that provides greater resistance at all ages. Sand was used as a fine aggregate with a quartz origin and was placed in an oven at 105 °C until reaching constant mass for the determination of the granulometric distribution (Figure 1), specific mass, and water absorption (Table 2).

Table 1. CP-II-F40 physical properties reported by the manufacturer.

Physical and Chemical Characteristics	
Density (g/cm^3)	3.16
Superficial area (m^2/g)	1.70
Initial setting time (min)	143
Initial setting time (min)	338
Water requirement (a/c)	0.30
Compressive Strength (MPa)	
1 day	25.20
3 days	36.20
7 days	39.80
28 days	47.40

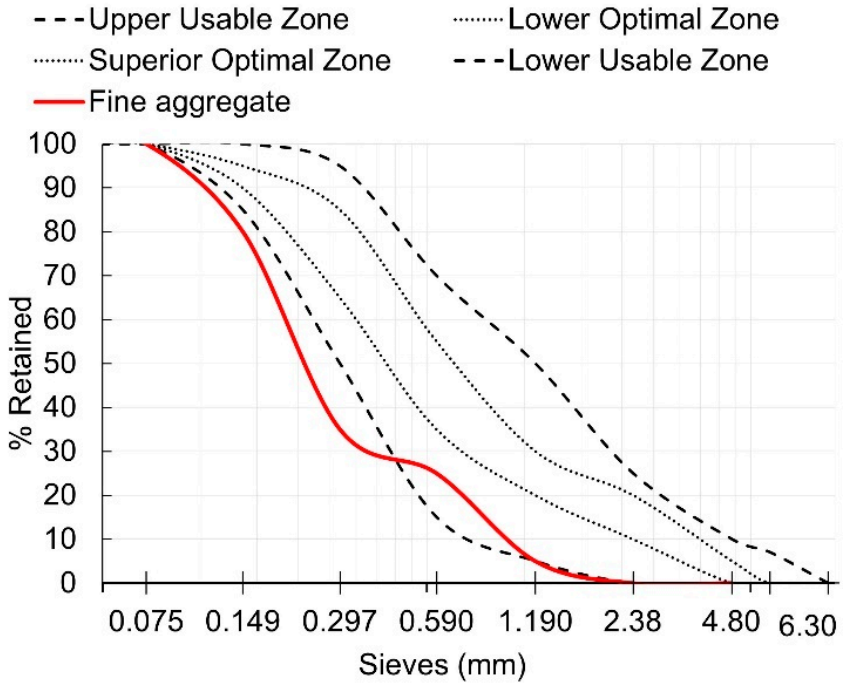

Figure 1. Sand granulometric distribution.

Table 2. Fine aggregate physical properties.

Physical Characteristics	
Maximum aggregate size (mm)	2.36
Fineness module	1.49
Density (g/cm^3)	2.61
Specific mass, wet surface (g/cm^3)	2.29
Water absorption (%)	5.91
Grain shape	Subrounded

Hydrated lime's (CH-I) specifications supplied by the manufacturer are presented in Table 3. The dregs used to substitute the lime were provided by the CMPC Celulose Rio-Grandense company, located in southern Brazil. This residue was dried in an oven at 105 °C for 24 h and ground in a ceramic ball mill for 5 h. The final granulometric distribution were analyzed via laser diffraction using Shimadzu model CILAS 1180 operating in a range from 0.04 to 2500 µm and a wavelength of up to 830 nm. The specific mass of Portland cement, lime, and dregs was determined according to NBR 16605 [14] and measured in a 250 cm^3 Le Chatelier flask utilizing kerosene with a specific mass of 0.752 g/cm^3. This liquid was also used because it is not reactive and has a lower specific mass than the analyzed powders.

Table 3. Chemical and physical properties of CH-I reported by the manufacturer.

Chemical Parameters (%)	
Moisture	0.00
Loss on ignition	24.52
Insoluble residue + SiO_2	5.37
CaO	42.07
MgO	28.04
Total oxides based on non-volatiles	92.89
Non-hydrated oxides	9.79
$Ca(OH)_2$ + $Mg(OH)_2$	73.93
CO_2	4.80
Combined H_2O	19.72
Residual carbonate (CO_3^{2-})	6.53
Physical Parameters	
#30 (0.60 mm)	0.00
#200 (0.0075 mm)	9.26

The materials were analyzed via thermogravimetry using a TGA-1000 equipment (Navas Instruments, Conway, NH, USA). In the test, temperature was changed from 20 °C (room temperature) to 1000 °C with a heating rate of 10 °C·min^{-1}. This test was executed to evaluate the thermal stability and volatile content of the raw materials according to the recommendations of the ASTM D7582 standard [15]. The infrared spectroscopy technique (FT-IR) was used in order to qualitatively evaluate the chemical characteristics of lime and dregs. For this, the tests were carried out in a Jasco spectrometer, model 4100, equipped with an attenuated total reflectance (ATR) device. The device was configured to perform 32 transmittance scans at a resolution of 4 cm^{-1} and readings between 4000 and 500 cm^{-1}. The dregs and lime were analyzed via X-ray diffraction (XRD) using the material passing through a sieve with an aperture of #325 mesh. The X-ray diffraction patterns were recorded using a D8 Advance diffractometer (Bruker, MA, USA) employing copper Kα radiation (λ = 0.15406 nm) and operating in the range of 5–75° 2θ, with a 0.05°/s temperature gradient and slots (slits) of $\frac{1}{2}$°. All tests applied to the raw materials were summarized in Table 4.

Table 4. Summary of characterization tests applied to the raw materials.

Test	**Analyzed Materials**	**Studied Property**
Laser diffraction	Sand and dregs	Granulometric distribution
Analysis of specific gravity, loose density, compacted density, and powdery material content	Cement, sand, lime, and dregs	Physical properties
Thermogravimetric analysis	Lime and dregs	Thermal stability and decomposition
X-ray Diffraction	Lime and dregs	Identification of material particles, clays, and other minerals.
Energy-dispersive X-ray spectroscopy	Cement, sand, lime, and dregs	Elemental analysis
Fourier-transform infrared spectroscopy	Lime and dregs	Identification of chemical compounds

2.2. Mixture Proportions, Sampling, and Curing

Mortar dosages were determined using the granulometric curve of the fine aggregate and the specific masses of the constituents according to Equations (1)–(3) [16]. Based on the results of energy dispersion X-ray spectroscopy and the chemical compatibility of lime with dregs, substitutions of 10%, 15%, 20%, and 30% were performed in relation to the hydrated lime mass (Table 5). The mixing procedure was performed in a planetary mortar

mixer, wherein the dry materials were mixed at low speed (140 rpm) for 30 s in order to homogenize the powders. Afterward, 75% of the water was added and mixed at high speed (220 rpm) for 60 s. Finally, the remaining water was added and mixed again at low speed (140 rpm) for another 60 s. Thereafter, the final amount of water was adjusted to ensure a consistency of 260 ± 10 mm in the flow table since consistencies above 270 mm generate types of mortar that were light, workable, and prone to exudation [17].

$$P_{sand} = 100 - \left[\left(1 - \frac{Yu}{Yr}\right) \times 100\right] \quad (1)$$

$$P_{cement} = 100 - (P_{lime} + P_{sand} + P_{water}) \quad (2)$$

$$P_{lime} = 100 - (P_{cement} + P_{sand} + P_{water}) \quad (3)$$

In the equations above, P_{sand} = fine aggregate content (%); P_{lime} = lime content (%); P_{cement} = cement content (%); Yu = dry-packed density of the fine aggregate (g/cm^3); and Yr = loose density of the fine aggregate (g/cm^3).

Table 5. Mixing proportion of the groups with respect to mass relation.

Group	Cement	Lime	Dregs	Sand	Water
0%	1.000	0.597	0.000	7.815	1.546
10%	1.000	0.537	0.060	7.815	1.560
15%	1.000	0.507	0.090	7.815	1.570
20%	1.000	0.477	0.120	7.815	1.580
30%	1.000	0.417	0.180	7.815	1.590

2.3. Fresh-State Properties

In the fresh state, the flowability of the mortar specimens was determined using a flow table test [18], wherein the fresh mortar was molded in a standardized cone and the flow was measured after 30 falls on the drop table. Specific gravity and air content tests (adapted from NBR 13278 [19]) were carried out to determine these properties in the fresh state using cylindrical molds with dimensions of 5 cm × 10 cm (diameter × length). Fresh mortar was poured into the mold; then, the mass was measured. The entrained air content was determined based on the fresh specific gravity and the actual specific gravity of the mortar. All tests applied to the fresh-state mortar specimens are summarized in Table 6.

Table 6. Summary of characterization tests applied to the mortar specimens in the fresh state.

Test	Studied Feature
Flow table	Granulometric distribution
Specific gravity	Physical property
Air content	Entrained air

2.4. Physical and Mechanical Properties

Physical properties of the hardened specimens, such as water absorption, void ratio, and density of the hardened types of mortar, were determined according to NBR 9778 [20]. Water absorption via capillarity, which describes the increase in moisture in cementitious composites in the hardened state, was determined according to NBR 15259 [21]. Water retention was determined according to NBR 13277 [22] using a modified Bucnher funnel with a vacuum pump, applying a suction of 51 mm of mercury for 15 min. All physical properties were determined using 15 prismatic specimens with dimensions of 4 cm × 4 cm × 16 cm (width × thickness × length) at 28 days of age. In this procedure, measurements of dimensions and mass were carried out using an analytical balance (0.1 g resolution) and analog caliper (0.01 mm resolution), respectively.

Three-point bending and compressive strength tests were executed in accordance with NBR 13279 [23]. Eight prismatic specimens were used per group, molded in the dimensions of 4 cm × 4 cm × 16 cm, and the tests were carried out at 28 and 56 days of age. The flexural test was carried out through a span of 10 cm and at a constant speed of 50 mm/min until the total rupture of the specimen, which fragmented into two pieces. Each piece was then evaluated under compression at a constant speed of 200 mm/min until they reached a new breaking point. Both mechanical tests were carried out on a universal mechanical testing machine (model DL 3000; brand—EMIC).

Tensile bond strength of the substrate was executed in small walls measuring approximately 0.48 m^2 (Figure 2a), and a cement and sand layer (Figure 2b) in a 1:3 ratio (cement: sand) was used to improve adhesion. Mortar specimens were prepared, and a single layer of 25 mm in thickness was applied to the walls for each group. After 28 days, tensile bond strength tests were carried out using a motorized drill equipped with a diamond cup saw with a diameter of 50 mm. Afterward, metal tabs approximately 5 cm in diameter were adhered to the walls with the aid of a two-component epoxy resin (Figure 2c). Before performing the mechanical tests, the resin was cured for 24 h at room temperature, i.e., the conditions reported by the supplier. The device used for manual hydraulic pullout was a Solotest with a capacity of 1500 kgf (Figure 2d), and the pullout strength was executed in accordance with NBR 13528-2 [22]. All tests applied to the hardened state were summarized in Table 7.

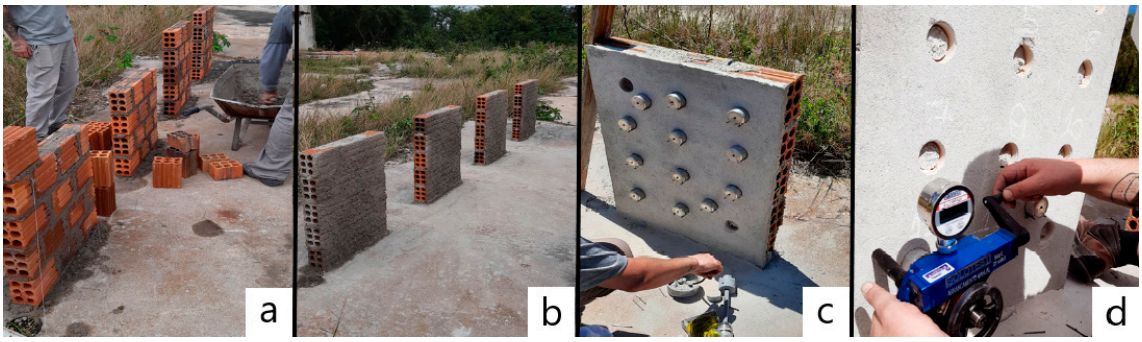

Figure 2. Photographs of the masonry walls (**a**), walls with applied adhesion substrate (**b**), walls with the mortar and metal tabs applied (**c**), and performance of the pullout test (**d**).

Table 7. Summary of characterization tests applied in the hardened state.

Test	Studied Feature
Water absorption, water retention, water absorption via capillarity, void ratio, and density	Physical properties
Three-point bending	Mechanical behavior
Compression	Mechanical behavior
Tensile bond strength	Mechanical behavior

2.5. Accelerated Aging Test

For the accelerated aging test, 56-day-old prismatic specimens with dimensions of 4 cm × 4 cm × 16 cm were subjected to 10 successive heating and cooling cycles, simulating the actions of bad weather during the life of a coating, as indicated by the NBR 15575-4 standard. Heating was performed in a laboratory oven set at 80 °C for approximately 60 min, and cooling was performed by spraying the specimens with water until they reached room temperature, which was monitored with the aid of an infrared thermometer. At the end of 10 heating/wetting cycles, the specimens were tested in terms of their compression and flexural tension using the procedures and equipment mentioned above.

2.6. Chemical Structure and Microscopy

The specimens' chemical compositions were measured via X-ray fluorescence (XFR) using a Rigaku RIX 2000. This is considered a non-destructive technique that allows for the identification of the chemical elements ($Z > 10$) present in a sample (qualitative analysis) and the establishment of the proportion (concentration) in which each element is present in a sample. For this test, the major elements, in their oxide forms (in significant concentrations), were chosen: SiO_2, Al_2O_3, Fe_2O_3 (total), MnO, MgO, CaO, Na_2O, K_2O, TiO_2, and P_2O_5. Mortar samples were taken for morphological analysis via scanning electron microscopy (SEM). SEM was performed using a Jeol model JSM 6060, which was made available by the Center for Microscopy and Microanalysis. A voltage of 5 kV, a working distance of 12.4 mm, and magnifications of 1800× and 3000× were used.

3. Results and Discussion

3.1. Physical and Chemical Characteristics of Lime and Dregs

Based on the obtained particle size distributions (Figure 3), it can be stated that the dregs have relatively fine granulometric properties with a unimodal distribution. The size distribution of these particles is very similar to that of lime, thereby allowing for the replacement of its fraction in the cement composite without modifying the pore distribution of the mortar. Since only a fraction of lime was substituted in this research, it is unlikely that the small difference between the granulometric curves changed the properties of the composite. Accordingly, Melo and co-workers [24] studied the production of lime with calcium-rich biomass ash and reported concentrations of 0.1% and 4% of materials retained in sieves with openings of 0.6 mm and 0.074 mm, respectively. Based on the pulp-and-paper production process, the small particle size attributed to the dregs can be ascribed to the presence of impurities, such as Na_2O, MgO, and SiO_2, which may have been incorporated into the dregs in the recovery of white liquor. Such a unimodal pattern and small average particle size have already been reported in the literature [25,26]. According to Novais and co-workers [26], the granulometry of ground dregs is similar to that of typical mortar pozzolans, such as metakaolin and fly ash.

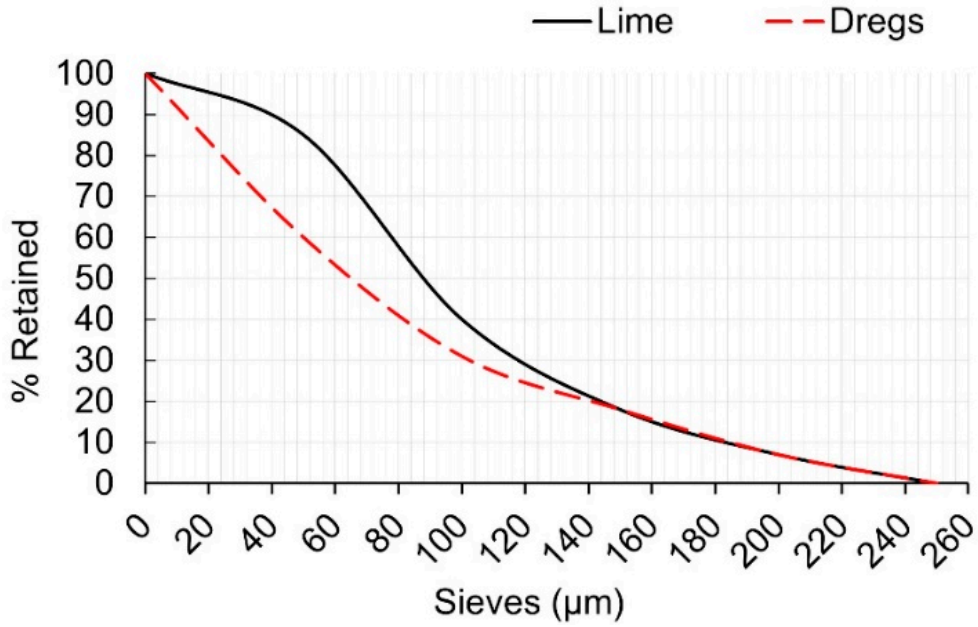

Figure 3. Particle size distribution of dregs and lime.

The levels of loose unit mass, compacted unit mass, and specific mass (Table 8) are within the limits reported in the literature for similar materials. Maheswaran and co-workers [27] studied a material they called lime mud, which appears to be equivalent to dregs since it comes from the recausticizing of green liquor. The authors observed

density and specific mass values of 0.616 g/cm^3 and 2.381 g/cm^3, respectively, with a moisture content of 52% and 85–90% of the material passing through a 40 µm sieve. It is important to note that the dregs were dried and ground in the present study, unlike the study by Maheswaran and co-workers [27], which explains the differences between the granulometries. Moreover, Moreira and co-workers [28] carried out a study on the incorporation of dregs in the clinker for the production of Portland cement and performed the drying, milling, and sieving of the residue, resulting in a specific mass of 2.44 g/cm^3 for a surface area of 1.03 m^2/g and a fineness index of 0.78%.

Table 8. Physical properties of materials.

Material	Loose Density (g/cm^3)	Compacted Density (g/cm^3)	Specific Gravity (g/cm^3)	Powdery Material Content (%)
Cement	1.11	1.19	2.93	-
Lime	0.58	0.71	2.35	99.10
Dregs	0.55	0.69	2.45	99.50
Sand	1.54	1.64	2.61	3.20

The diffractogram of the studied dregs (Figure 4) indicates the presence of a predominant phase of calcite ($CaCO_3$), which was expected due to the origin of the material; however, along with the presence of calcium ions, contamination from lignin was observed. Similarly, Santos and co-workers [25] found CaO within the dregs employed in their study, as it was the only compound to form crystalline phases and, therefore, easily detected in the X-ray diffractogram. According to the literature, the CaO content in dregs varies between 30 and 70% [25,27–29]. In addition, some studies reported levels of SiO_2 and SO_3 above 5% [25,27,28]. Several studies also indicated small traces of dolomite ($CaMg(CO_3)_2$) and cesanite ($Ca_2Na_3(SO_4)_3(OH)$) in addition to peaks indicating quartz (SiO_2), sodium carbonate (Na_2CO3), pyrsonite ($CaNa_2(CO_3)_2.2H_2O$), magnesium oxide (MgO), wustite (FeO), and calcium hydroxide ($Ca(OH)_2$) [25–29]. As in the work conducted by Santos and co-workers [25], in the present study, none of these crystalline structures were identified in the XRD spectra.

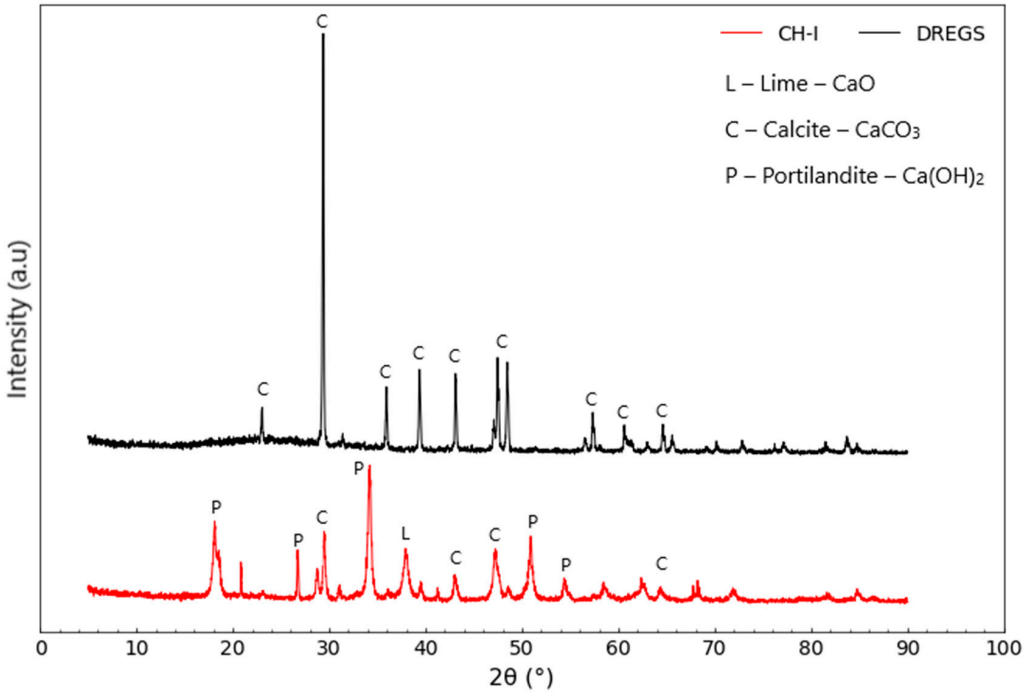

Figure 4. X-ray diffractogram of dregs and lime.

Typical compositions of the conventional building materials used in the present study were confirmed (Table 9). In this regard, it is important to note that the equipment used in this study does not detect the presence of certain elements, including carbon, hydrogen, and oxygen, which certainly conditioned the results obtained. However, the dominant presence of calcium in the lime and cement was verified, as well as the presence of silicon in the sand, which is in accordance with the literature [24]. The composition of the dregs also presented expected characteristics and was similar to that verified for lime, indicating that the partial replacement of lime by dregs is promising.

Table 9. Elemental composition of materials determined via EDX.

Element	Dregs	Lime	Cement	Sand
Ca	97.003	97.08	82.486	2.175
Si	1.137	1.423	8.413	75.975
Fe	0.333	0.703	5.088	1.768
K	0.216	0.631	1.479	7.083
Mn	0.418	0.087	0.108	-
Cu	0.057	0.04	0.037	0.029
Sr	0.527	0.036	0.207	0.028
S	0.19	-	1.758	-
Zn	0.061	-	0.066	0.026
Al	-	-	-	11.706
Others	0.058	-	0.355	1.211

Figure 5 shows the FTIR spectra obtained for dregs and lime. The signals at 710–715 cm^{-1} (in-plane bending vibration of CO_3^{2-} ions), 870–875 cm^{-1} (out-of-plane bending vibration of CO_3^{2-} ions), 1470 cm^{-1} (asymmetrical vibration deformation of CO_3^{2-} ions), and 1800 cm^{-1} (stretch vibration of C=O bonds) are typically reported for dregs in the literature [30]. The absence of bands in the range between 1070 cm^{-1} and 1080 cm^{-1} confirms that calcium carbonate was present in the form of calcite since the bonds representing this compound are inactive with respect to infrared radiation due to the symmetry of the calcium crystals [25]. The strong band in the region of 3300–3900 cm^{-1} observed for lime is associated with the vibration of OH bond stretching and indicates the presence of $Ca(OH)_2$ [31].

Regarding the thermogravimetric analysis of dregs and lime, Figure 6 shows a relatively stable pattern of their mass levels throughout the heating tests up to a temperature of 300 °C. Thus, fluctuations in the mass levels of these materials can be attributed to noise or inaccuracies of the equipment. Starting at 700 °C, the mass of the dregs decayed at an intense and constant level until 800 °C. Lime, on the other hand, showed this behavior between 300 and 400 °C and again between 600 and 700 °C. The 5–10% loss of the initial mass of the dregs occurring up to around 200 °C can be attributed to the water physically adsorbed in the material in addition to the dehydration of $CaSO_4$ [28]. Afterward, between 300 °C and 500 °C, an exothermic event occurred, which was likely related to the burning of organic compounds [32]. Between 500 °C and 800 °C, the observed thermal decomposition of the material may be associated with the decomposition of $CaCO_3$ and $MgCO_3$ [28]. In this regard, it is normal and expected that some elements verified in the dregs from other studies are not identified in the material analyzed in the present study since it is a heterogeneous residue originating from an industrial process with many variations, especially with respect to a comparison between waste from different industries. Between 800 °C and 1000 °C, the dregs experienced a mass loss of approximately 30%, which was probably related to the decomposition of calcium carbonate or calcite ($CaCO_3$), which transforms into CaO and CO_2 [27,28].

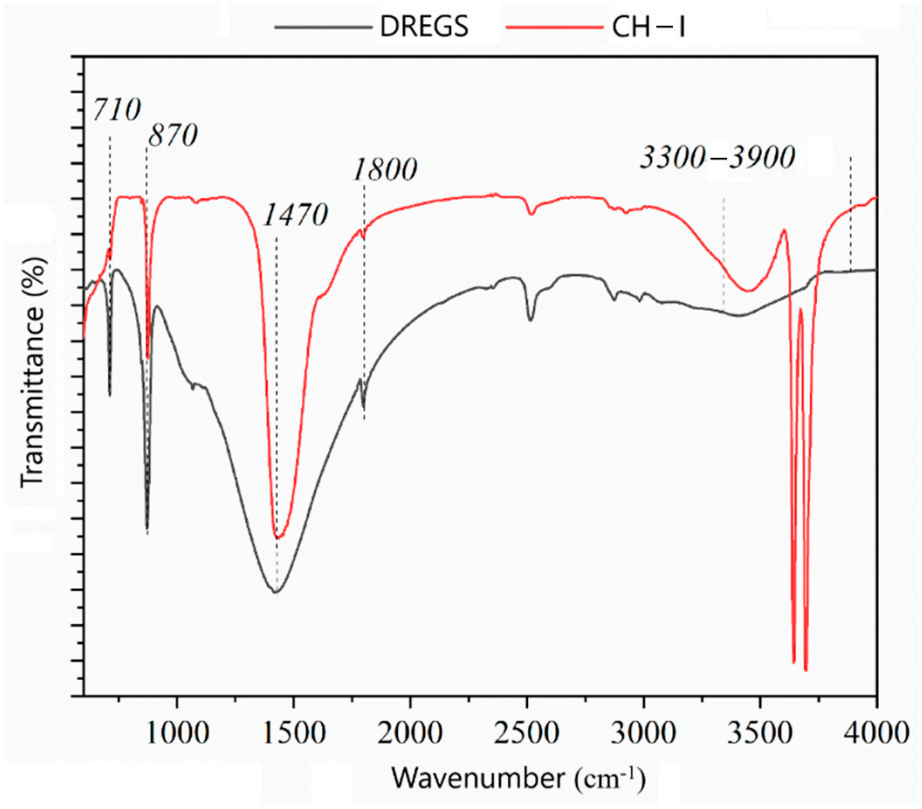

Figure 5. Infrared spectra of dregs and lime.

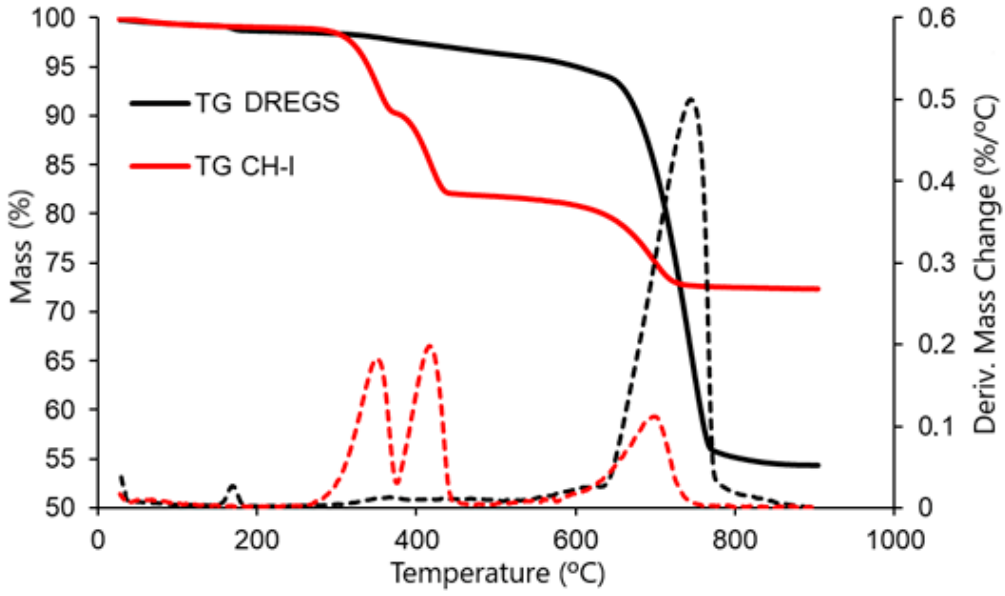

Figure 6. Thermal decomposition profiles of mortar components.

3.2. Physical Properties in Fresh and Hardened State

The specimens' density in the fresh state (Figure 7a) did not show variation upon the comparison of the types of mortar in this study (0.03% reduction rate), which may be attributed to the density of the dregs and lime being very similar. Regarding the incorporated air content (Figure 7b), there is no clear pattern of variability as a function of the content of added dregs; therefore, the similarity (3.96% reduction rate) between the average values indicates that the insertion of dregs did not confer any difference in rheological mechanisms that favored the formation of bubbles during the mixing of the mortar components and the consequent presence of pores filled with air. This similarity

was desired since incorporated air may enhance the workability of the paste; however, an increase in its content possibly represents a decrease in mechanical properties. All the composites studied showed a density in the fresh state between 1800 and 2200 kg/m^3 and can be classified in the same class according to NBR 13281 [33] (D5 group), which determines the requirements for the application of coating mortar on walls and ceilings.

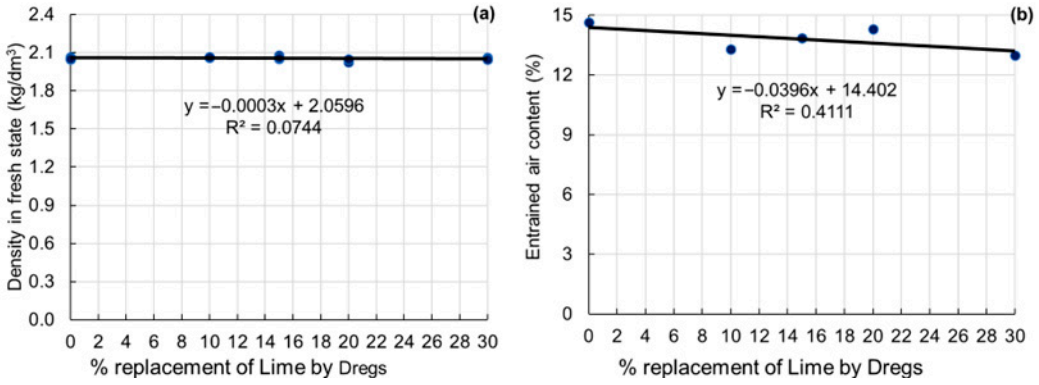

Figure 7. Density in the fresh state (**a**) and incorporated air content (**b**) of the types of mortar.

Similar to the fresh-state physical properties, the water absorption (0.92% reduction rate), void ratio (0.81% increase rate), and density in the hardened state (0.02% reduction rate) (Figure 8) of the specimens do not seem to differ when comparing the mortar specimens under study. This behavior is due to the aforementioned similarities between the dregs and the lime, including their density, granulometric characteristics, and chemical composition. The densities of the mortar specimens in the hardened state achieved the limits between of 1600 to 2000 kg/m^3 and can be classified in the same class according to NBR 13281 (M5 group) [33].

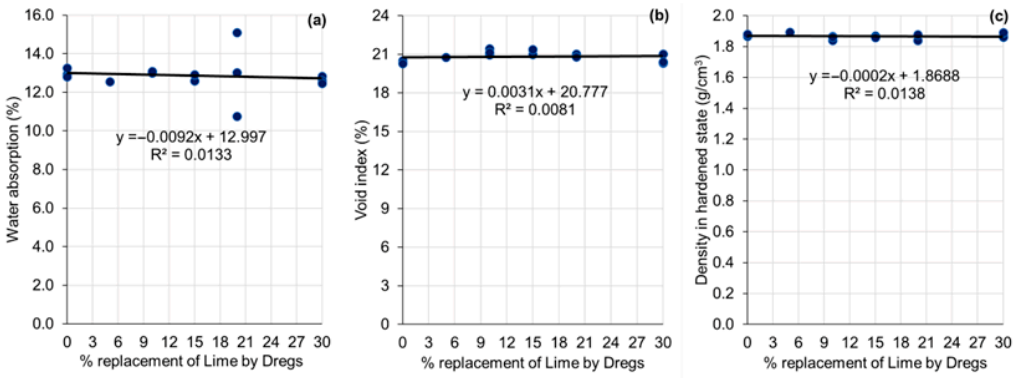

Figure 8. Water absorption (**a**), void ratio (**b**), and density (**c**) in the hardened state.

Furthermore, the water absorption via the capillarity coefficient increased (maximum 25.29% increase in 20% dregs) as the content of dregs increased (Figure 9). However, it is known that the phenomena related to capillarity are different when comparing mortar produced with and without hydrated lime [16,17,34]. In this sense, Marvila and co-workers [35] affirm that lime acts similarly to sand in relation to capillarity, increasing the absorption coefficient. When lime is used as a binder, capillarity cannot be fully explained based on the porosity of the mortar and the presence of capillary pores [17,34]. However, even though an increase in the capillarity coefficient was achieved with the use of the dregs, all the types of mortar studied presented a capillarity coefficient greater than 10 g/dm^2/min^2 and can be classified in the same class according to NBR 13281 (C6 group) [33], which is a high level of capillarity. This capillarity can reduce the useful life of the mortar due to the carrying of aggressive agents, however, it can allow the entry of CO_2 (CO_2 capture) and increase the mortar's mechanical resistance due to carbonation [34].

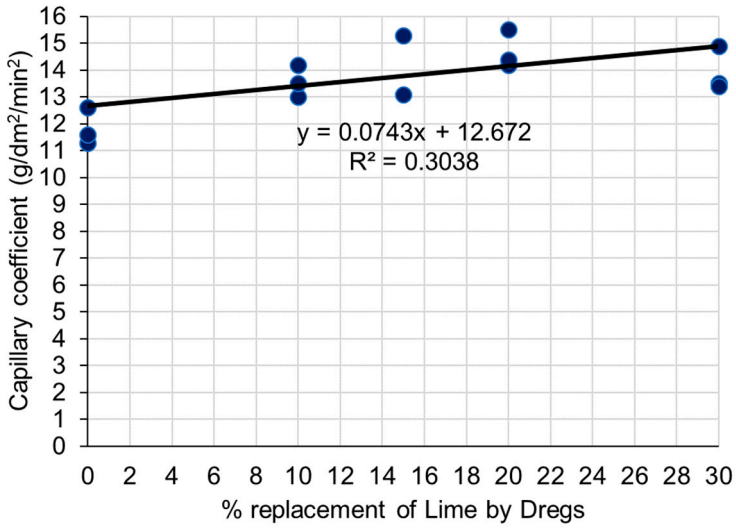

Figure 9. Capillary coefficient of mortar specimens.

3.3. Mechanical Properties

When comparing the mortar specimens at 28 and 56 days old, the results (Figure 10) indicate higher levels of compressive and flexional strength for the 56-day-old mortar specimens. These results were expected and can be attributed to the increase in the hydration level of the employed Portland cement in later ages. Furthermore, according to Bella and collaborators [36], mortar specimens composed of lime usually have relatively low levels of resistance for up to 56 days, as this resistance depends on the level of carbonation. This carbonation depends on the temperature of the environment, the moisture content in the pores of the mortar, and the concentration of CO_2 in the atmosphere to which the mortar is exposed [36]. Regarding the addition of dregs, the levels of compressive strength and flexural strength showed a stabilization trend after 28 days. These results again confirm the role of dregs as an agent capable of imitating the role of lime in mortar.

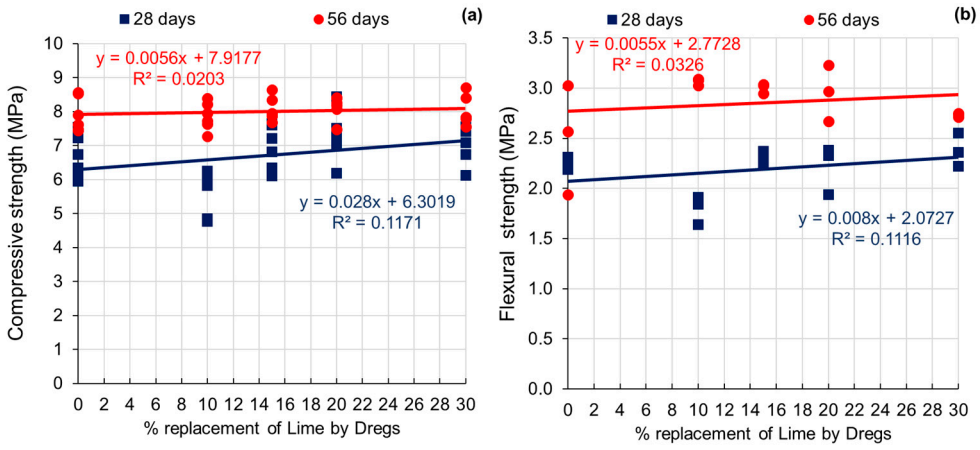

Figure 10. Compressive (**a**) and flexural (**b**) strengths of mortar specimens.

In addition, the pull-out strength obtained in this study was higher than those reported in recent research [37,38]. According to Silva and co-workers [39], the performance of mixed mortar specimens is superior to that of mortar entirely composed of pure cement or pure lime binders. The adhesion of the mortar is afforded by the penetration of the binder paste in the pores and the roughness of the substrate, wherein water retention capacity, consistency, air content, and mechanical strength are factors that interfere with adhesion [40]. Since the mortar specimens with and without dregs are very similar in terms of these properties, there were no differences between the studied mortar specimens (Figure 11). Regarding the

classification of the mortar specimens with respect to this property according to the current standards, all groups converged toward the highest resistance class (A3) [33].

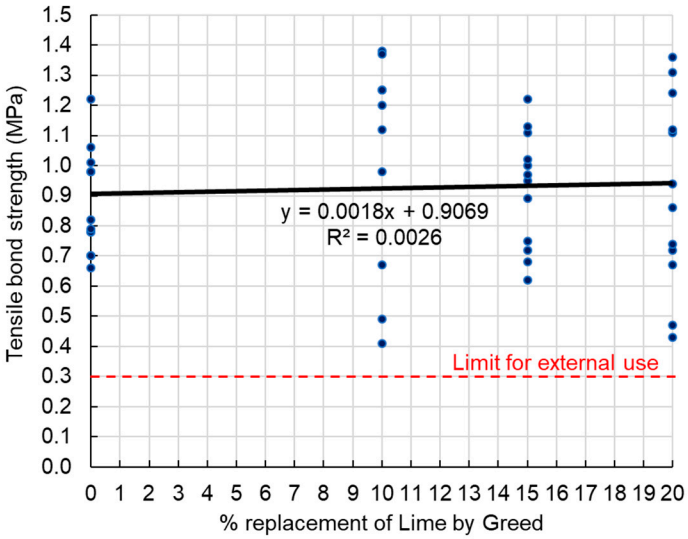

Figure 11. Mortar specimens' tensile bond strength.

3.4. Mortar Specimens' Chemical and Microstructural Properties

The chemical elements detected using X-ray fluorescence (XRF) via energy dispersive spectroscopy (EDX) for the studied mortar specimens are shown in Table 10, and their respective spectra are presented in Figure 12. Regarding the spectra, the detected peaks indicate the presence of typical cement compounds (Ca and Si), which are associated with hydrated silicates such as tricalcium silicate and dicalcium silicate [26,41]. There were also significant amounts of Fe and K present, which were associated with tetracalcium iron aluminate and potassium hydroxide, respectively [41].

Table 10. Elementary composition of mortar specimens determined via XRF.

Element	Concentration (%)				
	0%	**10%**	**15%**	**20%**	**30%**
Ca	75.229	71.532	66.396	71.397	71.101
Si	16.802	20.580	25.887	20.647	21.450
Fe	4.453	4.283	3.995	4.097	3.957
K	1.627	1.802	2.151	1.938	1.781
S	0.961	0.926	0.963	0.951	0.940
Ti	0.339	0.512	0.359	0.468	0.384
Others	0.589	0.366	0.248	0.502	0.386

Although the elemental compositions of the mortar specimens were strongly affected by the selection of material for analysis, it is possible to observe a reduction in the content of Ca and Fe in addition to an increase in the Si content as a consequence of the incorporation of sand and dregs. These results are relevant since the fractions of CaO and Fe_2O_3 are approximately 40–50% and 0.5–1%, respectively, according to the literature [29]. These fractions are lower when compared to mortar without the addition of dregs. Accordingly, it is not possible to attribute any difference in composition in terms of the content of dregs incorporated in the mortar specimens. However, the increase in the Si content attributed to the replacement of lime by dregs again indicates the presence of impurities, such as SiO_2, which was mentioned previously in this research.

The aggregate/matrix interface was similar in terms of porosity, and typical compounds (Portlandite and CSH) were visualized (Figure 13). The similarity between the

groups corroborates the mechanical properties and durability indicators, for which no significant variation was identified. In fact, it is known that the interfacial transition zone is the weakest region of a cementitious composite [42], and, as there was no change, this had an impact on the non-alteration of mechanical properties and durability between the different groups, regardless of the percentage of substitution.

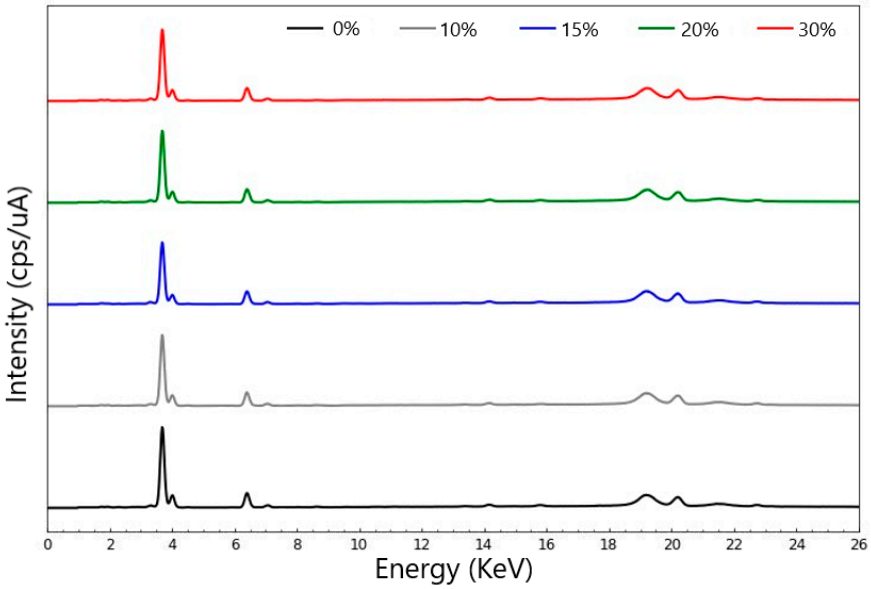

Figure 12. XRF spectra of mortar specimens.

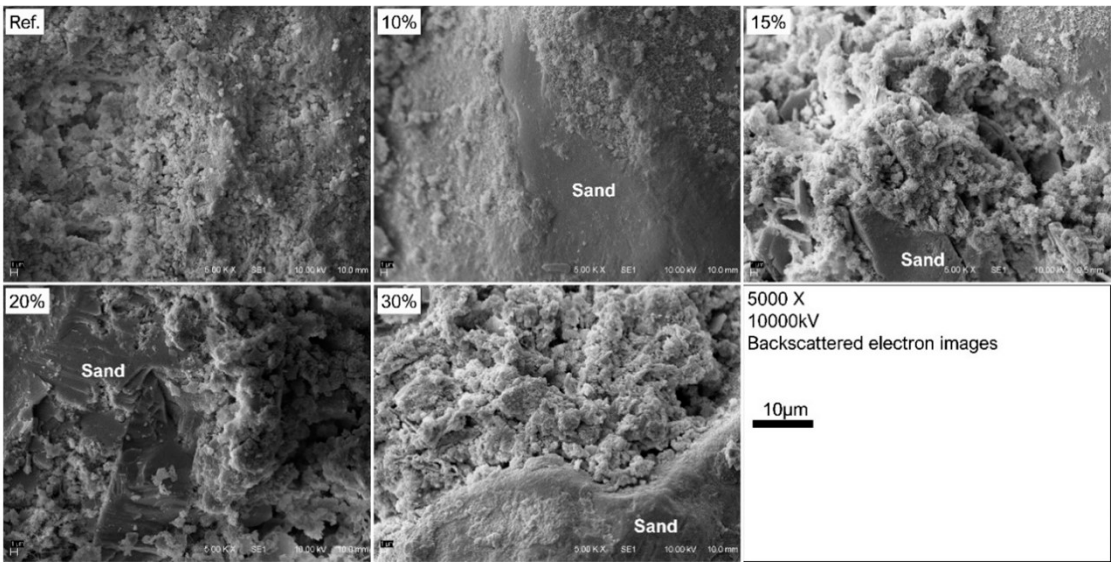

Figure 13. Scanning electron microscopy images of the control-mortar–Interfacial Transition Zone (ITZ).

Regarding the hydrated compounds in the cement matrix, once analyzed in the broken section, it was found that calcium hydroxide (Portlandite) was found in the samples at 10, 15, and 20%, and 30% of dregs (Figures 14 and 15), while Ref. did not detect Portlandite in the image. It is noteworthy that calcite ($CaCO_3$) morphologies (Figure 15) were found in both samples.

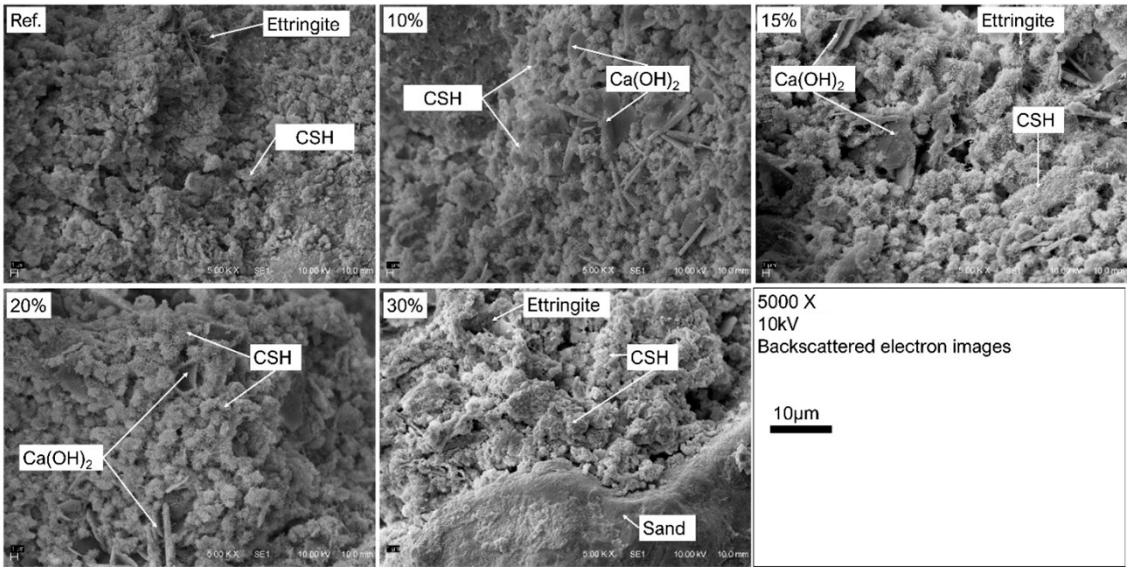

Figure 14. Scanning electron microscopy of the control-mortar–hydrated-cement compounds.

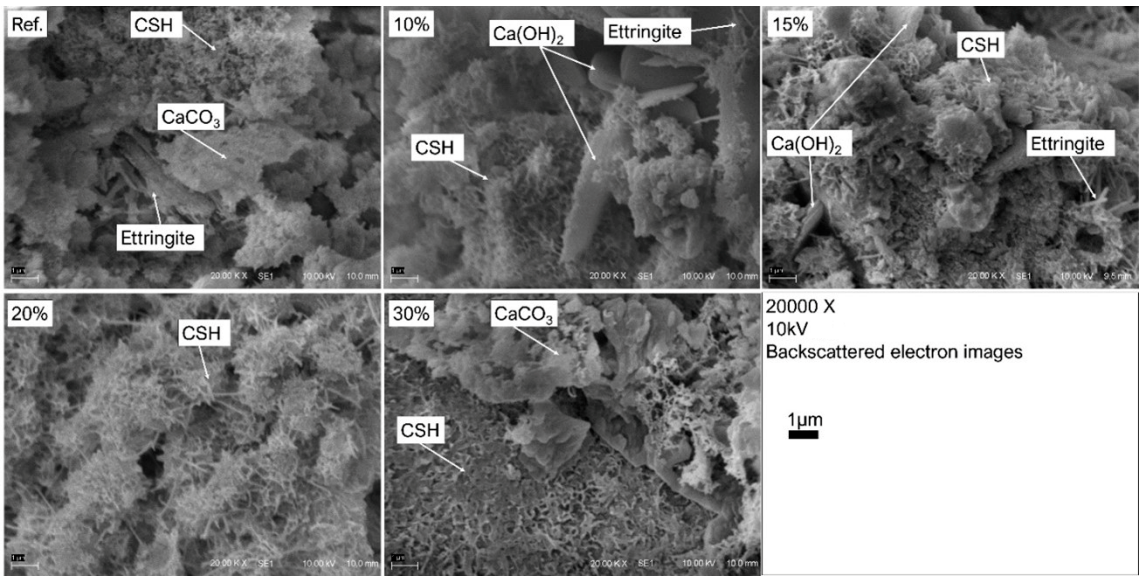

Figure 15. Scanning electron microscopy of the control mortar–hydrated cement compounds.

In general, it can be considered that the microstructure of Portland cement composites is marked by the formation of pores in the interfacial regions between the fine aggregate and the cement. Figures 13–15 confirm the presence of these pores, confirming the growth trend as the dregs content increased. In addition. it can be stated that the presence of dregs did not reduce the formation of hydrated calcium silicate crystals (C-S-H), which determine most of the physical and mechanical properties of Portland cement composites.

Correlating with mechanical properties, adhesion occurs by the mechanical interlocking of the cement hydration products (ettringite and CSH) transferred to the pores of the substrate. Ettringite ($3CaO.Al_2O_3.3CaSO_4.32H_2O$–hydrated calcium trisulfoaluminate) has a long, narrow rod shape of approximately 4–5 µm (Figures 14 and 15). It represents 20% to 25% of the volume of solids in a fully hydrated slurry [17,34,43]. The precipitation of ettringite is initiated when Portland cement is mixed with water, wherein gypsum is used as a regulating source of the cement setting time dissolving and releasing sulfate and calcium ions; these ions are the first to enter the solution, followed by aluminate and calcium ions from the dissolution of C_3A in the cement.

Due to the suction or capillary absorption effect induced by the porous base, relevant ions in the solution are transported to more internal regions of the substrate, where they form hydrated calcium trisulfoaluminate (ettringite) inside the pores [44]. Due to the faster dissolution processes of SO_4^{2-}, AlO_4^{-}, and Ca_2^{+} ions and ettringite precipitation, this product primarily fills capillary pores, which explains its greater abundance in the mortar/substrate contact zone and the surface pores of the base [17,43]. CSH, on the other hand, has a morphology that varies from poorly crystalline strands to a crystalline lattice (Figures 14 and 15). This phase constitutes about 50% to 60% of the solid volume of the fully hydrated pulp [17,34,43]

3.5. Aging Tests

The strength levels evaluated in terms of compressive (2.71% increase rate) and flexural strength (0.55% increase rate) (Figure 16) were similar to those verified for the same mortar specimens in the period prior to aging (56 days of age). In some cases, there were strength gains as a result of aging. A similar pattern of property gain after aging was reported by Ghiassi and Oliveira [45], who aged lime-based mortar specimens using freeze–thaw cycles. The authors justified their results based on the proposition of mechanisms beneficial to the mechanical properties that occurred during aging, which probably outweighed the damage caused by the severe conditions imposed. In this sense, it is possible to assume that the number of cycles adjusted in the present study might not have been large enough to induce more significant damage to the mortar specimens [46].

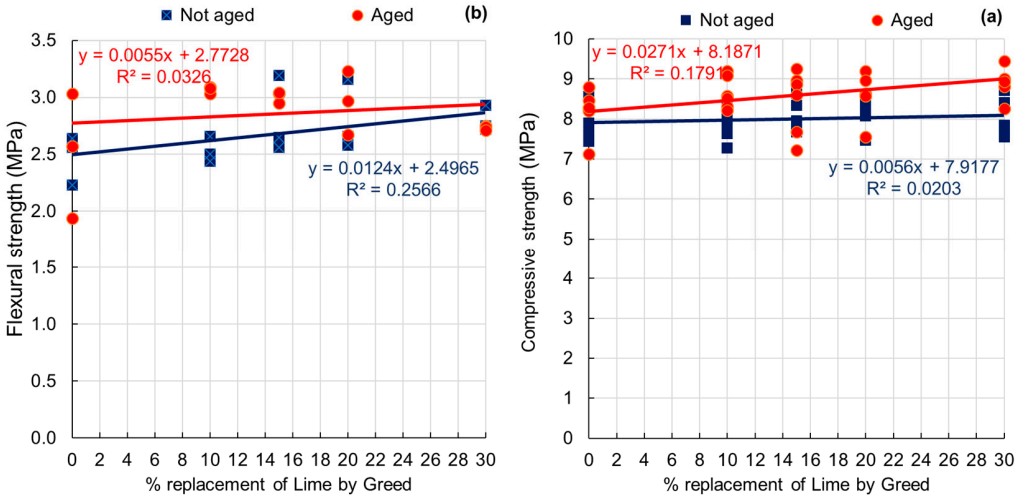

Figure 16. Compressive (**a**) and flexural (**b**) strength of aged and unaged mortar specimens.

4. Conclusions

The use of dregs from green liquor in cement composites can also contribute to the sustainability of the construction industry. By utilizing this waste product, the environmental impact of the pulp and paper industry can be reduced. In the present research, the following results were obtained:

- The replacement of lime by dregs in all the percentages studied did not impair the performance of the manufactured composites in terms of their rheological, physical, or mechanical characteristics;
- The green liquor dregs analyzed in the present study presented granulometric and chemical-composition-related properties similar to those CH-I lime;
- As a result of the abovementioned similarities, the patterns of variation in the properties evaluated for the mortar specimens in their fresh and hardened states showed a pattern of general similarity;
- The SEM images obtained indicated that the presence of dregs in the mortar specimens did not change the formational mechanism of C-S-H crystals, which explains the high degree of similarity of the properties evaluated in the fresh and hardened state.

These results are highly valuable as they allow for the conclusion that the new mortar specimens studied herein are viable and efficient without the use of additives, in addition to indicating that dregs can act in a similar way as lime in mixed mortar specimens. The possibility of the partial replacement of lime gives the dregs high added value and, in economic terms, can be an alternative for cost reduction and the mitigation of environmental impacts related to the use of CH-I lime. The durability of these composites will be addressed in further studies, including wetting/drying cycles and alkaline and sulfate attacks.

Author Contributions: Conceptualization A.I.d.O. and R.d.A.D.; methodology, A.I.d.O., H.L.R., G.H.T. and A.B.A.; software, A.B.A., G.H.T. and R.d.A.D.; validation, H.L.R., A.B.A. and W.J.d.S.; formal analysis, A.B.A., W.J.d.S. and R.d.A.D.; investigation, A.I.d.O., H.L.R. and G.H.T.; resources, M.S. and R.d.A.D.; data curation, H.L.R., A.B.A. and R.d.A.D.; writing—original draft preparation, A.I.d.O. and A.B.A.; writing—review and editing, A.I.d.O., W.J.d.S. and R.d.A.D.; visualization, A.I.d.O., A.B.A., W.J.d.S., M.S. and R.d.A.D.; supervision, W.J.d.S. and R.d.A.D.; project administration, R.d.A.D.; funding acquisition, M.S. and R.d.A.D. All authors have read and agreed to the published version of the manuscript.

Funding: This work was supported by Coordination for the Improvement of Higher Education—CAPES (code 001) and National Council for Scientific and Technological Development—CNPq (Financial codes 310413/2021-4 and 407560/2021-1).

Data Availability Statement: The data presented in this study are available on request from the corresponding author.

Acknowledgments: The authors gratefully acknowledge Coordination for the Improvement of Higher Education Personnel (CAPES) and the National Council for Scientific and Technological Development (CNPq) for their financial support.

Conflicts of Interest: The authors declare no conflict of interest.

References

1. Quina, M.J.; Pinheiro, C.T. Inorganic Waste Generated in Kraft Pulp Mills: The Transition from Landfill to Industrial Applications. *Appl. Sci.* **2020**, *10*, 2317. [CrossRef]
2. IBÁ Relatório Anual. 2020. Available online: https://iba.org/datafiles/publicacoes/relatorios/relatorio-iba-2020.pdf (accessed on 5 September 2022).
3. Rodrigues, L.R.; Francisco, M.A.C.O.; Sagrillo, V.P.D.; Louzada, D.M.; Entringer, J.M.S. Caracterização de resíduos sólidos da indústria de celulose tipo kraft visando sua aplicação no desenvolvimento de materiais cerâmicos. *22° CBECiMat Congr. Bras. Eng. Ciência Mater.* **2016**, *1*, 750.
4. Azevedo, A.R.G.; Alexandre, J.; Marvila, M.T.; Xavier, G.d.C.; Monteiro, S.N.; Pedroti, L.G. Technological and environmental comparative of the processing of primary sludge waste from paper industry for mortar. *J. Clean. Prod.* **2020**, *249*, 119336. [CrossRef]
5. Formaggio, A.R.; Formaggio, R.A.; Sanches, I.D. *Sensoriamento Remoto em Agricultura*, 1st ed.; Oficina de Textos: São Paulo, Brazil, 2017; ISBN 978-85-7975-277-3.
6. SÁNCHEZ, L.E. *Avaliação de Impacto Ambiental: Conceitos e Métodos*, 3rd ed.; Oficina de Textos: São Paulo, Brazil, 2020.
7. Wang, D.; Zhu, J.; He, F. CO_2 carbonation-induced improvement in strength and microstructure of reactive MgO-CaO-fly ash-solidified soils. *Constr. Build. Mater.* **2019**, *229*, 116914. [CrossRef]
8. Sewsynker-Sukai, Y.; Naomi David, A.; Gueguim Kana, E.B. Recent developments in the application of kraft pulping alkaline chemicals for lignocellulosic pretreatment: Potential beneficiation of green liquor dregs waste. *Bioresour. Technol.* **2020**, *306*, 123225. [CrossRef]
9. Liu, M.; Wu, H.; Yao, P.; Wang, C.; Ma, Z. Microstructure and macro properties of sustainable alkali-activated fly ash mortar with various construction waste fines as binder replacement up to 100%. *Cem. Concr. Compos.* **2022**, *134*, 104733. [CrossRef]
10. Ma, Z.; Shen, J.; Wang, C.; Wu, H. Characterization of sustainable mortar containing high-quality recycled manufactured sand crushed from recycled coarse aggregate. *Cem. Concr. Compos.* **2022**, *132*, 104629. [CrossRef]
11. Pasandín, A.R.; Pérez, I.; Ramírez, A.; Cano, M.M. Moisture damage resistance of hot-mix asphalt made with paper industry wastes as filler. *J. Clean. Prod.* **2016**, *112*, 853–862. [CrossRef]
12. Buruberri, L.H.; Seabra, M.P.; Labrincha, J.A. Preparation of clinker from paper pulp industry wastes. *J. Hazard. Mater.* **2015**, *286*, 252–260. [CrossRef]
13. *ABNT NBR 16697*; Portland Cement—Requirements. Brazilian Association of Technical Standards: Rio de Janeiro, Brazil, 2018; pp. 1–12.

14. *ABNT NBR 16605*; Portland Cement and Other Powdered Material—Determination of the Specific Gravity. Brazilian Association of Technical Standards: Rio de Janeiro, Brazil, 2017; pp. 1–4.
15. *ASTM D7582-15*; Standard Test Methods for Proximate Analysis of Coal and Coke by Macro Thermogravimetric Analysis. ASTM International: West Conshohocken, PA, USA, 2016; pp. 1–9. [CrossRef]
16. dos Santos, W.J.; Alvarenga, R.d.C.S.S.; Pedroti, L.G.; da Silva, R.C.; Freire, A.S.; de Moraes, B.A.; Carvalho, C.C. Proposta de método de dosagem para argamassas de revestimento com areia artificial de britagem. *Ambient. Construído* **2018**, *18*, 225–243. [CrossRef]
17. Souza, A.T.; Caldas, R.B.; Ludvig, P.; dos Santos, W.J. The effects of mixture's components on the mechanical properties and durability indicators of mixed mortar using simplex network method. *Constr. Build. Mater.* **2020**, *249*, 118740. [CrossRef]
18. *ABNT NBR 7215*; Portland Cement—Determination of Compressive Strength of Cylindrical Test Specimens. Brazilian Association of Technical Standards: Rio de Janeiro, Brazil, 2019; pp. 1–12.
19. *ABNT NBR 13278*; Mortars Applied on Walls and Ceilings—Determination of the Specific Gravity and The Air Entrained Content in the Fresh Stage. Brazilian Association of Technical Standards: Rio de Janeiro, Brazil, 2005.
20. *ABNT NBR 9778*; Hardened Mortar and Concrete—Determination of Absorption, Voids and Specific Gravity. Brazilian Association of Technical Standards: Rio de Janeiro, Brazil, 2005; pp. 1–4.
21. *ABNT NBR 15259*; Mortars Applied on Walls and Ceilings—Determination of Water Absorption Coefficient Due to Capilary Action. Brazilian Association of Technical Standards: Rio de Janeiro, Brazil, 2005; pp. 1–3.
22. *ABNT NBR 13277*; Mortars Applied on Walls and Ceilings—Determination of the Water Retentivity. Brazilian Association of Technical Standards: Rio de Janeiro, Brazil, 2005; pp. 1–3.
23. *ABNT NBR 13279*; Mortars Applied on Walls and Ceilings—Determination of the Flexural and the Compressive Strength in the Hardened Stage. Brazilian Association of Technical Standards: Rio de Janeiro, Brazil, 2005; pp. 1–9.
24. Melo, M.C.S.; Neves, G.A.; Menezes, R.R.; Ferreira, H.C.; Nóbrega, A.C.V.; Marinho, E.P. Cal produzida a partir de cinza de biomassa rica em cálcio. *Cerâmica* **2018**, *64*, 318–324. [CrossRef]
25. Ribeiro dos Santos, V.; Dezena Cabrelon, M.; de Sousa Trichês, E.; Quinteiro, E. Green liquor dregs and slaker grits residues characterization of a pulp and paper mill for future application on ceramic products. *J. Clean. Prod.* **2019**, *240*, 118220. [CrossRef]
26. Novais, R.M.; Carvalheiras, J.; Senff, L.; Labrincha, J.A. Upcycling unexplored dregs and biomass fly ash from the paper and pulp industry in the production of eco-friendly geopolymer mortars: A preliminary assessment. *Constr. Build. Mater.* **2018**, *184*, 464–472. [CrossRef]
27. Maheswaran, S.; Kalaiselvam, S.; Arunbalaji, S.; Palani, G.S.; Iyer, N.R. Low-temperature preparation of belite from lime sludge and nanosilica through solid-state reaction. *J. Therm. Anal. Calorim.* **2015**, *119*, 1845–1852. [CrossRef]
28. Torres, C.M.M.E.; Silva, C.M.; Pedroti, L.G.; Fernandes, W.E.H.; Ballotin, F.C.; Zanuncio, A.J.V. Dregs and grits from kraft pulp mills incorporated to Portland cement clinker. *J. Mater. Cycles Waste Manag.* **2020**, *22*, 851–861. [CrossRef]
29. Martínez-Lage, I.; Velay-Lizancos, M.; Vázquez-Burgo, P.; Rivas-Fernández, M.; Vázquez-Herrero, C.; Ramírez-Rodríguez, A.; Martín-Cano, M. Concretes and mortars with waste paper industry: Biomass ash and dregs. *J. Environ. Manage.* **2016**, *181*, 863–873. [CrossRef] [PubMed]
30. Xia, M.; Yao, Z.; Ge, L.; Chen, T.; Li, H. A potential bio-filler: The substitution effect of furfural modified clam shell for carbonate calcium in polypropylene. *J. Compos. Mater.* **2015**, *49*, 807–816. [CrossRef]
31. Cizer, Ö.; Rodriguez-Navarro, C.; Ruiz-Agudo, E.; Elsen, J.; Van Gemert, D.; Van Balen, K. Phase and morphology evolution of calcium carbonate precipitated by carbonation of hydrated lime. *J. Mater. Sci.* **2012**, *47*, 6151–6165. [CrossRef]
32. Simão, L.; Jiusti, J.; Lóh, N.J.; Hotza, D.; Labrincha, J.A.; Montedo, O.R.K. Waste-containing clinkers: Valorization of alternative mineral sources from pulp and paper mills. *Process Saf. Environ. Prot.* **2017**. [CrossRef]
33. *ABNT NBR 13281*; Mortars Applied on Walls and Ceilings—Requirements. Brazilian Association of Technical Standards: Rio de Janeiro, Brazil, 2005; pp. 1–7.
34. Haddad, L.D.d.O.; Neves, R.R.; de Oliveira, P.V.; dos Santos, W.J.; de Carvalho Junior, A.N.; dos Santos, W.J. Influence of particle shape and size distribution on coating mortar properties. *J. Mater. Res. Technol.* **2020**, *9*, 9299–9314. [CrossRef]
35. Marvila, M.T.; de Azevedo, A.R.G.; Ferreira, R.L.S.; Vieira, C.M.F.; de Brito, J.; Adesina, A. Validation of alternative methodologies by using capillarity in the determination of porosity parameters of cement-lime mortars. *Mater. Struct.* **2022**, *55*, 19. [CrossRef]
36. Di Bella, G.; Fiore, V.; Galtieri, G.; Borsellino, C.; Valenza, A. Effects of natural fibres reinforcement in lime plasters (kenaf and sisal vs. Polypropylene). *Constr. Build. Mater.* **2014**, *58*, 159–165. [CrossRef]
37. Branco, F.G.; Belgas, M.d.L.; Mendes, C.; Pereira, L.; Ortega, J.M. Mechanical performance of lime mortar coatings for rehabilitation of masonry elements in old and historical buildings. *Sustainability* **2021**, *13*, 3281. [CrossRef]
38. Andrejkovičová, S.; Velosa, A.L.; Rocha, F. Air lime–metakaolin–sepiolite mortars for earth based walls. *Constr. Build. Mater.* **2013**, *44*, 133–141. [CrossRef]
39. Silva, B.A.; Pinto, A.P.F.; Gomes, A. Influence of natural hydraulic lime content on the properties of aerial lime-based mortars. *Constr. Build. Mater.* **2014**, *72*, 208–218. [CrossRef]
40. Carasek, H. *Argamassas. Mater. construçao Civ. e Princípios Ciência dos Mater*, 1st ed.; IBRACON: São Paulo, Brazil, 2007; pp. 863–904, ISBN 978-85-98576-19-0.
41. Moghadam, M.A.; Izadifard, R.A. Effects of zeolite and silica fume substitution on the microstructure and mechanical properties of mortar at high temperatures. *Constr. Build. Mater.* **2020**, *253*, 119206. [CrossRef]

42. Almada, B.S.; Alves da Silva Neto, G.; Fraga do Prado, D.; Paulino Aguilar, M.T.; Silva Garcia, D.C.; Brigolini Silva, G.J.; José dos Santos, W. Evaluation of the microstructure and micromechanics properties of structural mortars with addition of iron ore tailings. *J. Build. Eng.* **2023**, *63*, 105405. [CrossRef]
43. Gulbe, L.; Vitina, I.; Setina, J. The Influence of Cement on Properties of Lime Mortars. *Procedia Eng.* **2017**, *172*, 325–332. [CrossRef]
44. Carasek, H. Argamassas. In *Materiais de Construção Civil e Princípios de Ciência e Engenharia de Materiais*; IBRACON: São Paulo, Brazil, 2007; pp. 863–904, ISBN 978-85-98576-27-5.
45. Dalalbashi, A.; Ghiassi, B.; Oliveira, D.V. Influence of freeze–thaw cycles on the pull-out response of lime-based TRM composites. *Constr. Build. Mater.* **2021**, *313*, 125473. [CrossRef]
46. Souza, A.T.; Alves, G.; Neto, S.; Neto, H.S.; Caldas, R.B.; Jose, W.; Santos, D. Evaluation of the mechanical performance of different coating mortars types after an accelerated aging process. *Aust. J. Basic Appl. Sci.* **2021**, *15*, 29–41.